Increasing extreme rainfall and rapid urbanisation major drivers behind Gaborone's deadly floods

Authors

Ben Clarke, *Centre for Environmental Policy, Imperial College, London, UK*
Mariam Zachariah, *Centre for Environmental Policy, Imperial College, London, UK*
Izidine Pinto, *Royal Netherlands Meteorological Institute (KNMI), De Bilt, The Netherlands*
Maja Vahlberg, *Red Cross Red Crescent Climate Centre, The Hague, the Netherlands; Swedish Red Cross, Stockholm, Sweden (based in Ubmeje/Umeå, Sweden)*
Vincent Pagiwa, *Okavango Research Institute, University of Botswana, Maun, Botswana*
Roop Singh, *Red Cross Red Crescent Climate Centre, The Hague, the Netherlands (based in New Jersey, USA)*
Nick Baumgart, *Copenhagen Centre for Disaster Research, Global Health Section, Department of Public Health, University of Copenhagen, Copenhagen, Denmark*
Emmanuel Raju, *Copenhagen Centre for Disaster Research, Global Health Section, Department of Public Health, University of Copenhagen, Copenhagen, Denmark; African Centre for Disaster Studies, North-West University, South Africa*
Karina Izquierdo, *Red Cross Red Crescent Climate Centre, The Hague, the Netherlands (based in Mexico City, Mexico)*
Stefaan Conradie, *Climate System Analysis Group & Environmental and Geographical Science Department, University of Cape Town, Cape Town, South Africa*
Tiro Nkemelang, *University of Cape Town, Cape Town, South Africa, Botswana Institute for Technology Research and Innovation, Gaborone, Botswana*
John Stegling, *Department of Meteorological Services Botswana, Gaborone, Botswana*
Piotr Wolski, *Climate System Analysis Group, University of Cape Town, Cape Town, South Africa*
Piet Kenbatho, *Department of Environmental Science*, *University of Botswana, Gaborone, Botswana*
Friederike Otto, *Centre for Environmental Policy, Imperial College, London, UK*

Review authors

Sjoukje Philip, *Royal Netherlands Meteorological Institute (KNMI), De Bilt, The Netherlands*
Sarah Kew, *Royal Netherlands Meteorological Institute (KNMI), De Bilt, The Netherlands*
Joyce Kimutai, *Centre for Environmental Policy, Imperial College, London, UK*
Lisa Thalheimer, *International Institute for Applied Systems Analysis, Laxenburg, Austria*

Main Findings

- During the rainy season Gaborone and other urbanised areas frequently experience flooding. High-intensity rainfall overwhelms drainage systems, often leading to significant urban flooding. The capital city's drainage infrastructure has not kept pace with its growing population density and rapid urbanisation rendering low-lying areas particularly susceptible to severe flooding events.
- Even in today's climate, which has warmed by 1.3 °C, the 5-day heavy rainfall event observed in February 2025 is relatively rare, expected to occur only once every 10 to-200 years, depending on the source of data. We use a 50-year return period for the remainder of the study. Analysing weather station data for Gaborone we find that the event has a return period of 40 years, meaning it has a 2-3% chance of occurring in any given year.
- To assess if human-induced climate change influenced the heavy rainfall in the region, we first determine if there is a trend in the observations, available since about 1950, that aligns with the pace of the earth's warming. Results show that observed 5-day rainfall events like that in February 2025 would have been much less likely to occur in a colder climate. Extrapolating this trend back to a 1.3 °C colder climate, this increase in intensity is estimated to be about 60%.
- To quantify the role of human-induced climate change we also analyse climate model data over the relatively small study region for the historical period. Overall, the available climate models show very different results. Some show a large increase in the frequency and intensity of extreme rainfall events, as in the observations, others show no change or even a decrease. This might be a result of climate change forcing in the models being comparable in strength with natural variability. Thus we cannot precisely quantify the role of climate change.
- When looking at a 2.6 °C warmer climate compared to preindustrial (the level of warming projected to occur later in the 21st century) we find that the majority of models show an additional increase in the magnitude of 5-day heavy rainfall events relative to 2025. This indicates the emergence of a climate change signal under higher warming levels.
- Taking together: (1) the very strong historical trend in all observed datasets; (2) the fact that warmer air can hold more water vapour which leads to a potential increase in rainfall intensity, and (3) the shift towards an increase in the majority of models with future warming, we conclude that human-induced climate change amplified the rainfall leading to flooding in southern Botswana, but cannot confidently quantify by how much.
- Considering that the majority of impacts of the February extreme weather event occurred due to flooding in urban areas, and that flooding often occurred historically, even under less extreme events, it is highly likely that those impacts were magnified by infrastructure not built to withstand such extreme rainfall. Roads, drainage channels, and dams were overwhelmed, while health clinics (e.g. in Molapowabojang and Kanye) faced severe disruptions.
- There are ongoing efforts to strengthen flood resilience through improved drainage,

land-use regulation, and disaster preparedness. Expanding drainage capacity, enforcing zoning to limit development in high-risk areas, and upgrading critical infrastructure to withstand both present and future climate challenges can further enhance resilience. A comprehensive approach that integrates multi-hazard assessments into urban planning, infrastructure development, and disaster preparedness, along with stronger early warning systems, can improve resilience to future extreme events.

1 Introduction

In mid February 2025, southern Botswana and eastern South Africa witnessed extreme rainfall (Fig. 1.1) leading to widespread flooding. At least 31 people were killed, with 22 fatalities in the KwaZulu-Natal region of South Africa, close to Durban, and nine in Botswana (Mhlophe-Gumede, 2025; Government of Botswana, 2025). The flooding also caused significant disruption across Botswana, affecting over 5000 people as well as leading to the closure of three ports of entry to South Africa, all government schools temporarily closed, and traffic disruptions leaving some areas of the country inaccessible.

The extreme rainfall began across arid and semi-arid areas of southern Botswana (and the eastern Kalahari Desert) from 15th February. Over the course of the next 5-6 days, this progressed eastwards, bringing extreme rainfall across the Limpopo River catchment, before moving into the uplands of eastern South Africa.

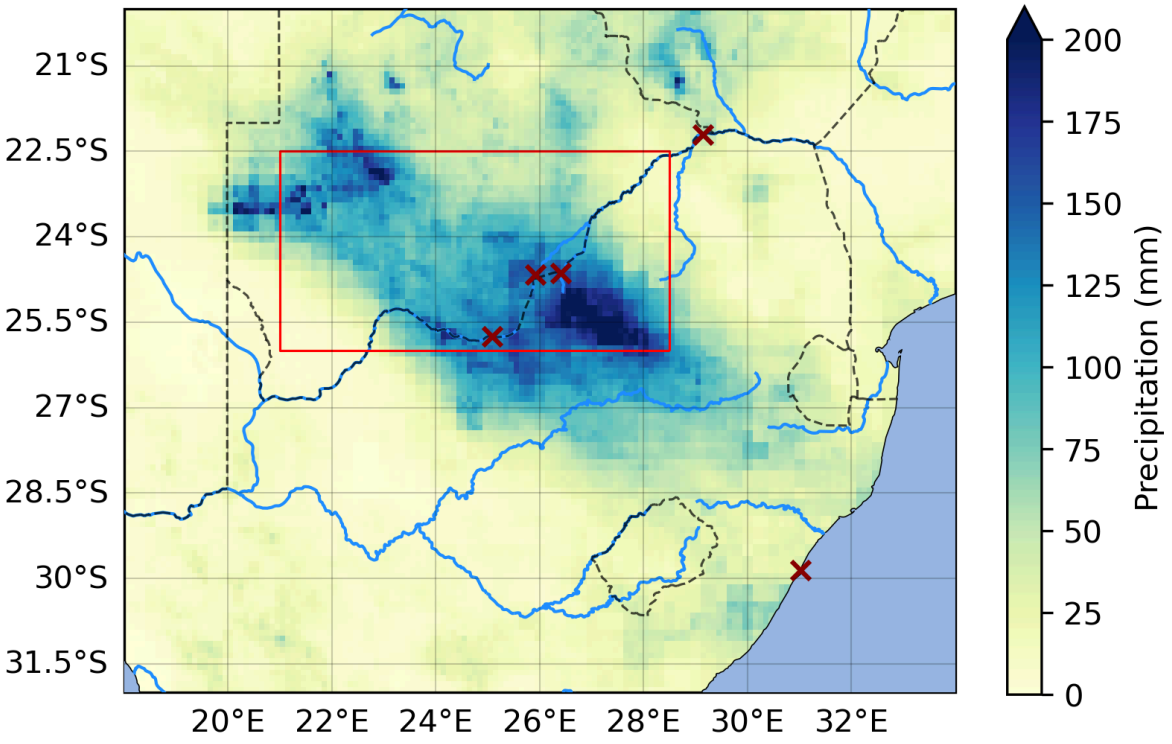

Figure 1.1: *5-day accumulated rainfall from 16-20th February 2025. Locations of reported impacts are shown by the dark red crosses, the study region is highlighted in red, and major rivers are shown in light blue. The Limpopo river passes along the border between Botswana and South Africa. Data from MSWEP (see section 2.1).*

Late on 14 February a deep, closed tropical low pressure system developed over far north-eastern Namibia. The system developed from an easterly wave trough in the mid-troposphere, which had tracked westward from Zimbabwe since 9 February. This trough represents the remnants of Tropical Storm Faida, which had made landfall over Mozambique, north-east of Beira on 8 February. The

upright tropical low strengthened over land on 15 February, while propagating slowly south-south-eastward. It was characterised by a warm core at 500hPa and strong ridge near the tropopause. Qualitatively this system resembles an Africáne (Viljoen et al., 2023), although it has not objectively been identified as such.

Qualitatively, the synoptic circulation associated with the system on 15 and 16 February 2025 relatively closely resembles the set up in mid-February 2017 (fig 1.2 top right). Then, an intense tropical low, identified as an Africáne (Viljoen et al., 2023), developed from the remnants of Tropical Cyclone Dineo, at roughly the same longitude, but about 2.5°N of the 2025 system (see Fig. 1.2 bottom right). In both cases a subtropical ridge extends from the Atlantic to Indian Oceans across South Africa to the south of the system, limiting the influence of the westerly wave on the movement and characteristics of the tropical low.

By the afternoon of 18 February, a high-amplitude westerly wave trough approached the western coastline of southern Africa, as the subtropical ridge split into Atlantic and Indian segments. This brought the tropical low under the steering influence of the westerly jet. The system appears to have disintegrated upon interaction with the high (~3000m) eastern escarpment on 19 February. Simultaneously, the westerly wave broke along South Africa's western coastline, yielding a cold-cored closed low off-shore of the South African-Namibian border. Together with the remnant moisture of the tropical low, the instability induced by the cold-cored low brought further moderate rainfall to parts of western Botswana on 20 and 21 February.

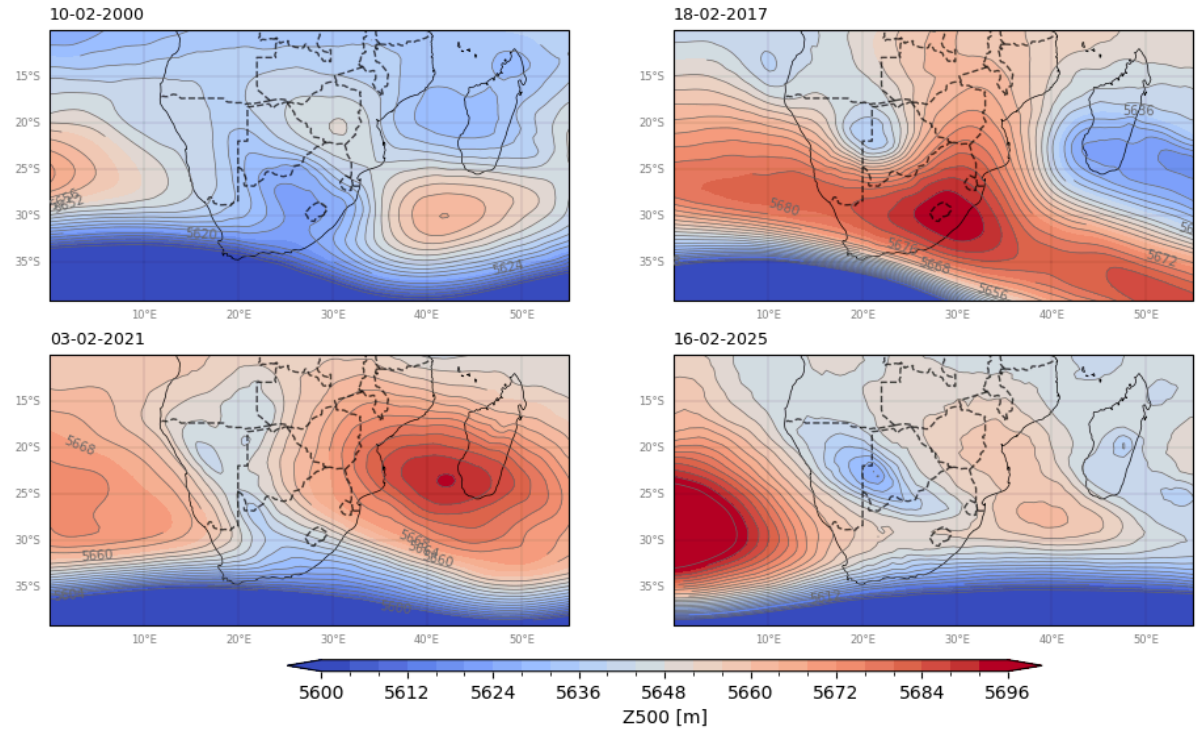

Figure 1.2: *Geopotential heights of 500 hPa pressure levels showing daily synoptic patterns during the event of interest (16th February 2025, bottom right) and other extreme precipitation events in the historical record in February 2000, 2017 and 2021. Data ERA5.*

The presence of a strong surface ridging anticyclone along southern Africa's east coast, in combination with widespread positive SST anomalies across the Mozambican Channel (cf. Mawren et

al., 2022) allowed for high levels of moisture transport along the Zambezi Valley and Limpopo Valley Low-Level Jets (Spavins-Hicks et al, 2021; Barimalala et al., 2021; Munday et al., 2020) subsequently converged on the eastern flank of the tropical low. Some moisture appears also to have been advected into the system from very anomalously warm waters off the central coast of Angola.

1.1 Rainfall extremes in Southern Africa and climate change

Working group 1 of the sixth assessment of the IPCC found increasing trends in extreme precipitation in both eastern and western Southern Africa (Seneviratne et al., 2021). In both regions, the attribution of this trend to anthropogenic climate change was considered low confidence due to a lack of any attribution studies. Since this synthesis, two studies on precipitation extremes affecting eastern coastal South Africa and Mozambique, as well as Malawi and Madagascar, were found to have been amplified by anthropogenic climate change (Otto et al., 2022; Pinto et al., 2022). However, no attribution studies exist for extreme precipitation in central or western southern Africa.

Several studies investigate changes in extreme precipitation indices with further warming. CMIP5 models project increases in the annual wettest day and wettest 5-day period across the semi-arid region encompassing southern central and eastern Botswana at warming levels of 1.5 and 2 C (Nkemelang et al., 2018). Consistent with this finding, studies using CORDEX models showed significant intra-regional variation; while there was no significant change over southeastern and southwestern Botswana, there were significant increases in extreme precipitation indices in the central and northwestern regions by the end of the century and amplified for greater global warming levels (Pinto et al., 2016; Akinyemi & Abiodun, 2019). Finally, McBride et al. (2022) indicate that extreme rainfall events have intensified over most of South Africa during the past 100 years, including those regions falling within the study domain along the border with Botswana.

Given the emerging consensus that precipitation extremes are intensifying in the region and that they are projected to increase with future warming, albeit with sub-regional variation, further exploration is urgent. An attribution study can help to disentangle the roles of anthropogenic climate change, vulnerability and exposure in driving the impacts that people experienced.

1.2 Event Definition

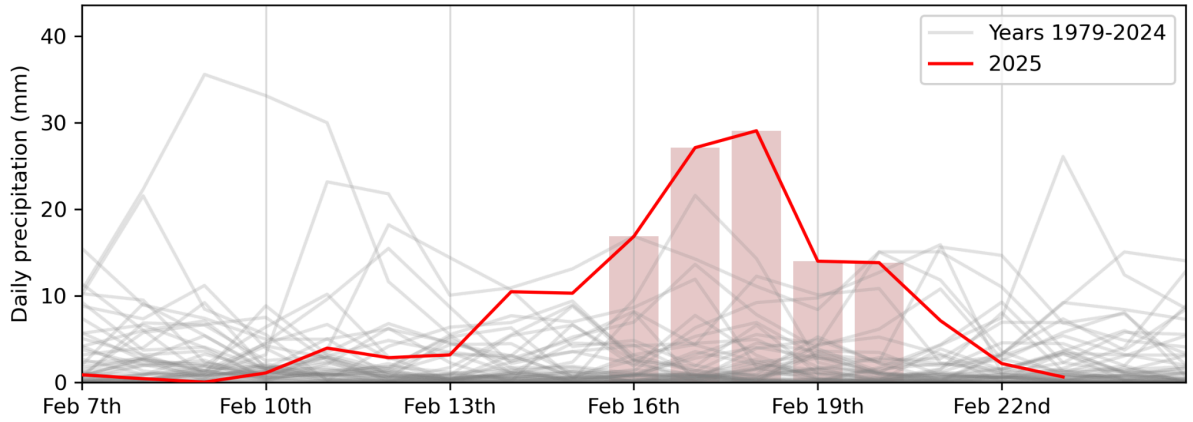

Figure 1.3: *Daily accumulated rainfall over southern Botswana through February 2025 (in red) and prior years in the record (in grey), averaged over the study region shown in figure 1.1. The days that form the event definition are highlighted by red bars. Data from MSWEP (see section 2.1).*

Impacts from this rainfall event were observed in Gaborone, at several border-crossing points along the Botswana-South Africa border, and in the Durban region of coastal South Africa (Fig. 1.1). For the latter, shown as the southeasternmost red 'x', the rainfall did not appear to be extreme in any of the gridded observational products used, suggesting that it occurred at prohibitively small spatial scales (for a rapid attribution analysis) and/or was due to a combination of heavy rainfall and very wet antecedent conditions. It was likely also driven by different meteorology. Furthermore, prior analysis in this region showed that annual maxima of extreme 2-day precipitation in the KwaZulu-Natal and Eastern Cape provinces have become roughly 4-8% more intense, and equivalently doubled in likelihood, due to anthropogenic climate change (Pinto et al., 2022). We therefore do not analyse extreme precipitation in southeastern South Africa in this study.

Meanwhile, Gaborone and all border crossing points are situated along the Limpopo River. However, given the limited run-off in this semi-arid and arid catchment, which makes up part of the Kalahari Desert, it was determined that analysing changes in extreme precipitation over the broader region of southern Botswana was more relevant to the observed impacts. Therefore, in order to capture the rainfall that led to impactful flooding, we study the 5-day annual maximum (from July-June each year, to account for the dry summer) extreme precipitation averaged over a region bounded by 21-28.5 °E, 22.5-26 °S), henceforth referred to as 'rx5day'.

In this report, we study the influence of anthropogenic climate change by comparing the likelihood and intensity of similar rx5day extremes at present with those in a 1.3 °C cooler climate. We also extend this analysis into the future by assessing the influence of a further 1.3 °C of global warming from present. This is in line with the latest Emissions Gap Report from the United Nations Environment Programme, which shows that the world is on track for at least 2.6 °C temperature rise given currently implemented policies (UNEP, 2024).

2 Data and methods

2.1 Observational data

In this study we use four observational and reanalysis datasets, as well as a local weather station, to study changes over time in rx5day extreme precipitation in the study region:

1. The European Centre for Medium-Range Weather Forecasts's 5th generation reanalysis product, ERA5, is a gridded dataset that combines historical observations into global estimates using advanced modelling and data assimilation systems (Hersbach et al., 2020). We use daily precipitation data from this product at a resolution of 0.25 .
2. The Multi-Source Weighted-Ensemble Precipitation (MSWEP) v2.8 dataset (updated from Beck et al., 2019) is fully global, available at 3-hourly intervals and at 0.1° spatial resolution, available from 1979 to ~3 hours from real-time. This product combines gauge-, satellite-, and reanalysis-based data.

3. The rainfall product developed by the UC Santa Barbara Climate Hazards Group called "Climate Hazards Group InfraRed Precipitation with Station data" (CHIRPS; Funk et al. 2015). Daily data are available at 0.05° resolution, from 1981-31 January 2025. The product incorporates satellite imagery with in-situ station data.
4. TAMSAT (Tropical Applications of Meteorology using SATellite and ground based observations, Maidment et al., (2017)), a daily rainfall dataset based on using high-resolution thermal-infrared observations to identify precipitating clouds. Daily rainfall data are available at 0.0375° x 0.0375° spatial resolution over the African continent from 1983 to the present.
5. Gaborone Met H.Q. (037-GABO) weather station - we use the daily precipitation totals from this weather station from 1925-2025. The station is located at 25.92 °E, 24.67 °S, and altitude 938 m.

Finally, as a measure of anthropogenic climate change we use the (low-pass filtered) global mean surface temperature (GMST), where GMST is taken from the National Aeronautics and Space Administration (NASA) Goddard Institute for Space Science (GISS) surface temperature analysis (GISTEMP, Hansen et al., 2010 and Lenssen et al. 2019).

2.2 Model and experiment descriptions

We use 2 multi-model ensembles from climate modelling experiments using very different framings (Philip et al., 2020): Sea Surface temperature (SST) driven global circulation high resolution models and regional climate models.

1. Coordinated Regional Climate Downscaling Experiment (CORDEX)-Africa (0.44° resolution, AFR-44) and Coordinated Regional Climate Downscaling Experiment CORDEX-CORE (0.22° resolution, AFR-22) multi-model ensembles (Nikulin et al., 2012; Giorgi and Gutowski, 2015; Giorgi et al., 2021), comprising of 32 simulations resulting from pairings of 10 Global Climate Models (GCMs) and 9 Regional Climate Models (RCMs). These simulations are composed of historical simulations up to 2005, and extended to the year 2100 using the RCP8.5 scenario.
2. HighResMIP SST-forced model ensemble (Haarsma et al. 2016), the simulations for which span from 1950 to 2050. The SST and sea ice forcings for the period 1950-2014 are obtained from the 0.25° x 0.25° Hadley Centre Global Sea Ice and Sea Surface Temperature dataset that have undergone area-weighted regridding to match the climate model resolution (see Table B).

2.3 Statistical methods

Methods for observational and model analysis and for model evaluation and synthesis are used according to the World Weather Attribution Protocol, described in Philip et al., (2020), with supporting details found in van Oldenborgh et al., (2021), Ciavarella et al., (2021) and here. The key steps, presented in sections 3-6, are: (3) trend estimation from observations; (4) model validation; (5) multi-method multi-model attribution; and (6) synthesis of the attribution statement.

In this report we analyse time series of 5-day annual maxima of precipitation averaged over a region around southern Botswana. For each time series we calculate the return period and intensity of the

event under study for the 2025 GMST and for 1.3 C cooler GMST: this allows us to compare the climate of now and of the preindustrial past (1850-1900, based on the Global Warming Index), by calculating the probability ratio (PR; the factor-change in the event's probability) and change in intensity of the event.

A nonstationary generalised extreme value (GEV) distribution is used to model 5-day extreme precipitation over a region around southern Botswana. For precipitation, the distribution is assumed to scale exponentially with the covariates, with the dispersion (the ratio between the standard deviation and the mean) remaining constant over time. This formulation reflects the Clausius Clapeyron relation, which implies that precipitation scales exponentially with temperature (Trenberth et.al., 2003, O'Gorman and Schneider 2009). The statistical models are estimated as follows. The variable of interest is assumed to follow a GEV distribution in which the location and scale parameters vary with GMST:

$$X \sim GEV(\mu, \sigma, \xi \mid \mu_0, \sigma_0, \alpha, T),$$

where X denotes the variable of interest, annual maxima of precipitation; T is the smoothed GMST; μ_0, σ_0 and ξ are the location, scale and shape parameters of the nonstationary distribution; and α is the trend due to GMST. As a result, the location and scale of the distribution have a different value in each year, determined by the GMST states. Maximum likelihood estimation is used to estimate the model parameters, with

$$\mu = \mu_0 exp\left(\frac{\alpha T}{\mu_o}\right) \quad \text{and} \quad \sigma = \sigma_0 exp\left(\frac{\alpha T}{\mu_o}\right).$$

3 Observational analysis: return period and trend

3.1 Analysis of point station data and gridded data

By fitting the statistical model described above to each observational time series (Figs 3.1 & 3.2), we estimate the return period of the 2025 event (Table 3.1). The gridded products give a wide range of estimates for the return period, from 8 years in TAMSAT and 22 years in MSWEP to nearly 250 years in ERA5. In part this results from the higher magnitude event estimated by ERA5. The local weather station in Gaborone showed a return period in the middle, at around 40 years. As a result of this wide variation, we elected to study changes in the 50 year event. While not tied directly to a single dataset, this is a useful benchmark for risk analysis. The 50 year event in CHIRPS gives an event of comparable magnitude to most of the other gridded estimates, reinforcing this proposal.

Dataset	5-day extreme precipitation		Change due to +1.3 °C GMST	
	Magnitude (mm)	Return period (95% C.I.)	Probability Ratio	Change in magnitude (%)
ERA5	142.17	244.86 (21.67 - inf)	Inf (2.12 - inf)	64.95 (4.87 - 125.13)
MSWEP	100.88	22.12 (6.61 - inf)	3.87 (0.009 - inf)	31.11 (-30.35 - 129.58)
TAMSAT	96.67	7.76 (3.25 - 110.76)	110.01 (3.31 - inf)	99.01 (15.90 - 229.21)
CHIRPS	99.03	50	47.89 (0.93 - inf)	58.52 (2.98 - 160.93)
Gaborone station (Met H.Q.)	240.1	37.29 (11.36 - 388.51)	3.20 (0.50 - 34.27)	24.22 (-11.14 - 65.39)

Table 3.1: *Estimated return periods of the 5-day extreme precipitation event over southern Botswana in the three observational datasets with coverage of the event, ERA5, MSWEP and TAMSAT, as well as the local weather station. The 50-year event is shown for the only dataset not including the event, CHIRPS. The change in probability ratio and magnitude due to increasing GMST for each time series are also shown. Light blue indicates an increasing trend that crosses no change, while dark blue indicates a statistically significant increasing trend.*

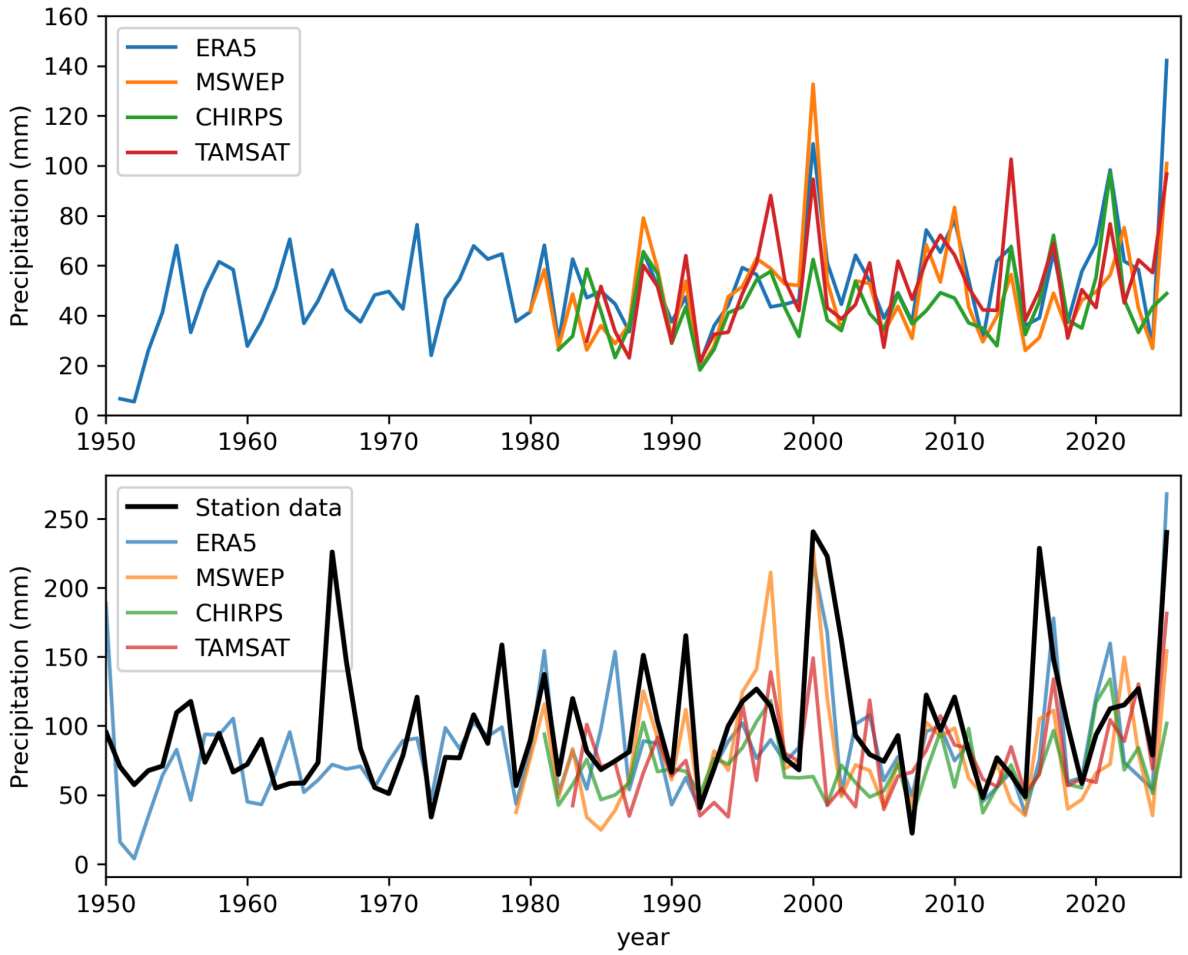

Figure 3.1: *Time series of 5-day annual maximum precipitation over southern Botswana (upper) and in Gaborone (lower) in observational and reanalysis datasets, from 1950-present. To calculate the Gaborone time series in gridded products, the closest grid point to the weather station (at 25.92 °E, 24.67 °S) was selected.*

All observational datasets used in this study give strongly increasing trends in the rx5day index due to current warming of 1.3 °C, both at the region scale and at the scale of a single grid point or weather station (Table 3.1, Fig. 3.1, Fig. A.1). ERA5 and TAMSAT give statistically significant increases in probability ratio and intensity, of infinity and 110, respectively, suggesting that such an event would have been extremely unlikely (return period of > 5000 years) if not impossible in a world without anthropogenic warming. MSWEP, CHIRPS and the local station give strong increases that are not significant at the 95% level, largely due to high variability, that vary between a 3- and 50-fold increase. Similarly, the intensity of a 50-year return period event has been observed to increase from 25-100%, with all estimates far exceeding the direct thermodynamic influence of ~7% per °C of warming.

Overall, the historical record shows a very strong increase in the frequency severity of such extremes. However, this must be combined with independent model analysis to give a complete attribution. Furthermore, uncertainties for individual datasets are very large, suggesting that model analysis is also needed to refine this estimate.

4 Model evaluation

In this section we show the results of the model evaluation for the assessed region. The climate models are evaluated against the observations in their ability to capture:

1. Seasonal cycles: For this, we qualitatively compare the seasonal cycles based on model outputs against observations-based cycles (Figs A.2 & A.3). We discard the models that exhibit ill-defined peaks in their seasonal cycles. We also discard the model if the rainy season onset/termination varies significantly from the observations.

2. Spatial patterns: Models that do not match the observations in terms of the large-scale precipitation patterns (Figs A.4 & A.5) are excluded.

3. Parameters of the fitted statistical models. We discard the model if the model and observation parameters ranges do not overlap.

The models are labelled as ‘good’,’reasonable’, or ’bad’ based on their performances in terms of the three criteria discussed above (Table 4.1). A model is given an overall rating of ‘good’ if it is rated ‘good’ for all three characteristics. If there is at least one ‘reasonable’, then its overall rating will be ‘reasonable’ and ‘bad’ if there is at least one ‘bad’. The tables show the model evaluation results. In this study, given the relatively large number of models available, only models whether ranked ‘good’ or those with only a single ‘reasonable’ are used for the final analysis.

Model / Observations	**Seasonal cycle**	**Spatial pattern**	**Dispersion**	**Shape parameter**	**Statistical properties**	**Conclusion (include? Y/N)**
CHIRPS			0.287 (0.207 ... 0.343)	0.022 (-0.32 ... 0.41)		
ERA5			0.404 (0.305 ... 0.484)	-0.19 (-0.46 ... 0.0054)		
MSWEP			0.356 (0.266 ... 0.407)	0.099 (-0.32 ... 0.51)		
TAMSAT			0.328 (0.245 ... 0.380)	0.011 (-0.37 ... 0.29)		
HighResMIP						
CMCC-CM2-HR4_highresSST (1)	reasonable	reasonable	0.160 (0.114 ... 0.198)	0.0043 (-0.68 ... 0.43)	bad	bad (N)
CMCC-CM2-VHR4_highresSST (1)	reasonable	good	0.255 (0.196 ... 0.301)	-0.034 (-0.27 ... 0.18)	good	reasonable (Y)
CNRM-CM6-1_highresSST (1)	good	reasonable	0.263 (0.191 ... 0.308)	0.056 (-0.29 ... 0.29)	good	reasonable (Y)
CNRM-CM6-1-HR_highresSST (1)	good	good	0.340 (0.256 ... 0.417)	-0.44 (-0.88 ... -0.26)	good	good (Y)
EC-Earth3P_highresSST (1)	good	reasonable	0.215 (0.149 ... 0.272)	-0.077 (-0.66 ... 0.41)	good	reasonable (Y)

EC-Earth3P-HR_highresSST (1)	good	reasonable	0.258 (0.190 ... 0.307)	-0.20 (-0.42 ... 0.00071)	good	reasonable (Y)
HadGEM3-GC31-HM_highresSST (1)	good	good	0.264 (0.179 ... 0.315)	0.030 (-0.20 ... 0.29)	good	good (Y)
HadGEM3-GC31-LM_highresSST (1)	good	reasonable	0.319 (0.226 ... 0.382)	-0.20 (-0.42 ... 0.051)	good	reasonable (Y)
HadGEM3-GC31-MM_highresSST (1)	good	reasonable	0.245 (0.181 ... 0.297)	-0.17 (-0.72 ... 0.023)	good	reasonable (Y)
MPI-ESM1-2-HR_highresSST (1)	good	reasonable	0.229 (0.157 ... 0.273)	-0.071 (-0.44 ... 0.34)	good	reasonable (Y)
MPI-ESM1-2-XR_highresSST (1)	good	reasonable	0.253 (0.192 ... 0.302)	-0.37 (-0.80 ... 0.19)	good	reasonable (Y)
CORDEX						
AFR-22_CanESM2_r1i1p1_CanRCM4 (1)	reasonable	reasonable	0.201 (0.145 ... 0.234)	-0.073 (-0.36 ... 0.27)	reasonable	reasonable (N)
AFR-22_HadGEM2-ES_r1i1p1_CCLM5-0-15 (1)	good	reasonable	0.270 (0.186 ... 0.330)	-0.12 (-0.45 ... 0.059)	good	reasonable (Y)
AFR-22_HadGEM2-ES_r1i1p1_RegCM4-7 (1)	reasonable	reasonable	0.155 (0.115 ... 0.184)	-0.16 (-0.50 ... 0.18)	bad	bad (N)
AFR-22_HadGEM2-ES_r1i1p1_REMO2015 (1)	good	good	0.252 (0.195 ... 0.300)	-0.066 (-0.40 ... 0.16)	good	good (Y)
AFR-22_MPI-ESM-LR_r1i1p1_CCLM5-0-15 (1)	good	good	0.292 (0.216 ... 0.338)	-0.22 (-0.54 ... 0.034)	good	good (Y)
AFR-22_MPI-ESM-LR_r1i1p1_REMO2015 (1)	reasonable	reasonable	0.268 (0.204 ... 0.315)	-0.11 (-0.30 ... 0.11)	good	reasonable (N)
AFR-22_MPI-ESM-MR_r1i1p1_RegCM4-7 (1)	reasonable	reasonable	0.223 (0.153 ... 0.274)	-0.19 (-0.41 ... 0.086)	good	reasonable (N)
AFR-22_NorESM1-M_r1i1p1_CCLM5-0-15 (1)	good	reasonable	0.223 (0.145 ... 0.276)	-0.098 (-0.40 ... 0.25)	good	reasonable (Y)
AFR-22_NorESM1-M_r1i1p1_RegCM4-7 (1)	bad	reasonable	0.154 (0.114 ... 0.193)	-0.18 (-0.55 ... 0.061)	bad	bad (N)
AFR-22_NorESM1-M_r1i1p1_REMO2015 (1)	reasonable	good	0.214 (0.158 ... 0.256)	-0.33 (-0.62 ... -0.13)	good	reasonable (Y)
AFR-44_CanESM2_r1i1p1_CanRCM4 (1)	good	reasonable	0.177 (0.134 ... 0.209)	0.011 (-0.50 ... 0.38)	reasonable	reasonable (N)

AFR-44_CanESM2_r1i1p1_RCA4 (1)	good	reasonable	0.223 (0.155 ... 0.268)	-0.044 (-0.26 ... 0.20)	good	reasonable (Y)
AFR-44_CNRM-CM5_r1i1p1_CCLM4-8-17 (1)	good	reasonable	0.215 (0.137 ... 0.269)	-0.17 (-0.45 ... 0.22)	good	reasonable (Y)
AFR-44_CNRM-CM5_r1i1p1_RCA4 (1)	good	reasonable	0.210 (0.164 ... 0.244)	-0.020 (-0.37 ... 0.24)	good	reasonable (Y)
AFR-44_CSIRO-Mk3-6-0_r1i1p1_RCA4 (1)	good	reasonable	0.224 (0.168 ... 0.273)	-0.066 (-0.44 ... 0.22)	good	reasonable (Y)
AFR-44_EC-EARTH_r12i1p1_CCLM4-8-17 (1)	good	reasonable	0.230 (0.165 ... 0.274)	-0.013 (-0.34 ... 0.31)	good	reasonable (Y)
AFR-44_EC-EARTH_r1i1p1_RACMO22T (1)	good	reasonable	0.181 (0.106 ... 0.216)	0.070 (-0.40 ... 0.45)	reasonable	reasonable (N)
AFR-44_EC-EARTH_r1i1p1_RCA4 (1)	good	reasonable	0.214 (0.166 ... 0.251)	0.17 (-0.047 ... 0.43)	good	reasonable (Y)
AFR-44_EC-EARTH_r3i1p1_HIRHAM5 (1)	bad	reasonable	0.257 (0.197 ... 0.304)	-0.021 (-0.27 ... 0.25)	good	bad (N)
AFR-44_GFDL-ESM2M_r1i1p1_RCA4 (1)	good	reasonable	0.213 (0.168 ... 0.250)	-0.35 (-0.62 ... -0.14)	good	reasonable (Y)
AFR-44_HadGEM2-ES_r1i1p1_CCLM4-8-17 (1)	good	reasonable	0.264 (0.201 ... 0.322)	0.038 (-0.46 ... 0.46)	good	reasonable (Y)
AFR-44_HadGEM2-ES_r1i1p1_GER-REMO2009 (1)	reasonable	reasonable	0.241 (0.187 ... 0.286)	-0.051 (-0.37 ... 0.21)	good	reasonable (N)
AFR-44_HadGEM2-ES_r1i1p1_RACMO22T (1)	good	good	0.180 (0.128 ... 0.209)	0.021 (-0.27 ... 0.31)	reasonable	reasonable (Y)
AFR-44_HadGEM2-ES_r1i1p1_RCA4 (1)	good	reasonable	0.234 (0.177 ... 0.280)	-0.27 (-0.67 ... -0.092)	good	reasonable (Y)
AFR-44_IPSL-CM5A-LR_r1i1p1_GER-REMO2009 (1)	reasonable	good	0.278 (0.189 ... 0.328)	-0.14 (-0.52 ... 0.28)	good	reasonable (Y)
AFR-44_IPSL-CM5A-MR_r1i1p1_RCA4 (1)	good	reasonable	0.277 (0.211 ... 0.325)	-0.37 (-0.67 ... -0.15)	good	reasonable (Y)
AFR-44_MIROC5_r1i1p1_GER-REMO2009 (1)	reasonable	reasonable	0.188 (0.139 ... 0.224)	-0.21 (-0.51 ... 0.031)	reasonable	reasonable (N)
AFR-44_MIROC5_r1i1p1_RCA4 (1)	reasonable	reasonable	0.198 (0.151 ... 0.236)	-0.087 (-0.47 ... 0.12)	reasonable	reasonable (N)

AFR-44_MPI-ESM-LR_r1i1p1_CCLM4-8-17 (1)	good	reasonable	0.328 (0.248 ... 0.391)	-0.37 (-0.73 ... -0.055)	good	reasonable (Y)
AFR-44_MPI-ESM-LR_r1i1p1_RCA4 (1)	good	reasonable	0.248 (0.195 ... 0.284)	-0.0033 (-0.29 ... 0.26)	good	reasonable (Y)
AFR-44_MPI-ESM-LR_r1i1p1_REMO2009 (1)	reasonable	reasonable	0.217 (0.159 ... 0.260)	-0.0096 (-0.22 ... 0.24)	good	reasonable (N)
AFR-44_NorESM1-M_r1i1p1_RCA4 (1)	reasonable	reasonable	0.189 (0.129 ... 0.229)	-0.15 (-0.53 ... 0.10)	reasonable	reasonable (N)

Table 4.1: *Evaluation results of the climate models considered for attribution analysis of rx5day. For each model, the threshold for a 1-in-50-year event is shown, along with the best estimates of the Dispersion and Shape parameters are shown, along with a 95% confidence intervals. Furthermore evaluation of the seasonal cycle and spatial pattern are shown in the appendix.*

5 Multi-method multi-model attribution

Model / Observations	Event magnitude	Current warming level [1.3 ˚C]		Future warming level [2.6 ˚C]	
		Probability ratio PR [-]	Change in intensity ΔI [%]	Probability ratio PR [-]	Change in intensity ΔI [%]
CHIRPS	99.028 mm	48 (0.93 ... 6.5e+6)	59 (3.0 ... 1.6e+2)		
ERA5	142.1705 mm	3.6e+8 (2.1 ... 1.7e+33)	65 (4.9 ... 1.3e+2)		
MSWEP	100.881 mm	3.9 (0.0086 ... 3.6e+8)	31 (-30 ... 1.3e+2)		
TAMSAT	96.66869 mm	1.1e+2 (3.3 ... 4.0e+6)	99 (16 ... 2.3e+2)		
HighResMIP	**Threshold for return period 50 yr**				
CMCC-CM2-VHR4_highresSST (1)	1.3e+2 mm	4.8 (0.48 ... ∞)	16 (-9.6 ... 50)		
CNRM-CM6-1_highresSST (1)	86 mm	0.24 (0.040 ... 1.4)	-20 (-40 ... 6.7)		
CNRM-CM6-1-HR_highresST (1)	87 mm	1.3 (0.073 ... ∞)	3.0 (-26 ... 41)		
EC-Earth3P_highresSST (1)	79 mm	0.57 (0.059 ... ∞)	-4.0 (-30 ... 28)		
EC-Earth3P-HR_highresSST (1)	86 mm	2.1 (0.21 ... ∞)	5.3 (-14 ... 30)		
HadGEM3-GC31-HM_highresSST (1)	1.2e+2 mm	0.89 (0.12 ... 8.7)	-1.4 (-25 ... 31)		
HadGEM3-GC31-LM_highresSST (1)	1.0e+2 mm	0.23 (0.055 ... 3.2)	-14 (-33 ... 7.9)		
HadGEM3-GC31-MM_highresSST (1)	1.0e+2 mm	0.25 (0.064 ... 2.7)	-15 (-31 ... 5.0)		
MPI-ESM1-2-HR_highresST (1)	1.0e+2 mm	1.1 (0.16 ... 2.2e+3)	1.1 (-21 ... 27)		
MPI-ESM1-2-XR_highresST (1)	89 mm	0.092 (0.033 ... 0.37)	-29 (-44 ... -10)		
CORDEX					

AFR-22_HadGEM2-ES_r1i1p1_CCLM5-0-15 (1)	83 mm	1.0 (0.28 ... 7.2)	0.21 (-14 ... 17)	1.0 (0.39 ... 2.4)	0.14 (-9.1 ... 8.4)
AFR-22_HadGEM2-ES_r1i1p1_REMO2015 (1)	96 mm	0.57 (0.11 ... 77)	-6.2 (-24 ... 20)	2.3 (1.0 ... 5.5)	7.6 (0.12 ... 15)
AFR-22_MPI-ESM-LR_r1i1p1_CCLM5-0-15 (1)	79 mm	0.15 (0.051 ... 0.95)	-19 (-33 ... -0.37)	0.11 (0.00034 ... 0.72)	-15 (-30 ... -2.6)
AFR-22_NorESM1-M_r1i1p1_CCLM5-0-15 (1)	1.0e+2 mm	0.90 (0.13 ... 18)	-1.1 (-20 ... 22)	1.7 (0.55 ... 4.9)	5.7 (-6.1 ... 16)
AFR-22_NorESM1-M_r1i1p1_REMO2015 (1)	1.1e+2 mm	1.0 (0.054 ... ∞)	0.059 (-24 ... 27)	1.4 (0.14 ... 4.8)	2.4 (-6.3 ... 10)
AFR-44_CanESM2_r1i1p1_RCA4 (1)	77 mm	0.56 (0.19 ... 1.7)	-5.4 (-16 ... 4.5)	1.4 (0.71 ... 3.1)	3.5 (-3.9 ... 10)
AFR-44_CNRM-CM5_r1i1p1_CCLM4-8-17 (1)	1.2e+2 mm	3.5 (0.36 ... ∞)	11 (-9.3 ... 36)	2.0 (0.79 ... 5.9)	6.3 (-2.2 ... 14)
AFR-44_CNRM-CM5_r1i1p1_RCA4 (1)	94 mm	0.63 (0.17 ... 4.8)	-5.8 (-23 ... 16)	0.90 (0.38 ... 2.2)	-1.3 (-12 ... 9.4)
AFR-44_CSIRO-Mk3-6-0_r1i1p1_RCA4 (1)	89 mm	0.74 (0.097 ... 8.4)	-3.3 (-25 ... 25)	0.36 (0.033 ... 1.3)	-9.1 (-23 ... 2.4)
AFR-44_EC-EARTH_r12i1p1_CCLM4-8-17 (1)	1.1e+2 mm	0.59 (0.14 ... 5.3)	-6.9 (-24 ... 16)	0.63 (0.22 ... 1.7)	-5.4 (-16 ... 5.4)
AFR-44_EC-EARTH_r1i1p1_RCA4 (1)	1.1e+2 mm	1.7 (0.63 ... 4.9)	8.1 (-6.2 ... 25)	2.1 (0.96 ... 3.8)	8.5 (-0.43 ... 17)
AFR-44_GFDL-ESM2M_r1i1p1_RCA4 (1)	85 mm	1.1 (0.15 ... ∞)	0.94 (-15 ... 19)	2.3 (0.78 ... 6.1)	8.6 (-1.6 ... 18)
AFR-44_HadGEM2-ES_r1i1p1_CCLM4-8-17 (1)	1.1e+2 mm	0.83 (0.18 ... ∞)	-1.8 (-21 ... 34)	2.1 (0.88 ... 6.3)	6.5 (-1.4 ... 14)
AFR-44_HadGEM2-ES_r1i1p1_RACMO22T (1)	70 mm	0.36 (0.11 ... 1.4)	-11 (-22 ... 4.1)	1.0 (0.54 ... 1.9)	-0.034 (-6.3 ... 6.6)
AFR-44_HadGEM2-ES_r1i1p1_RCA4 (1)	91 mm	1.4 (0.35 ... 18)	2.9 (-10 ... 17)	2.1 (1.1 ... 4.3)	7.6 (0.77 ... 14)

AFR-44_IPSL-CM5A-LR_r1i1p1_GER-REMO2009 (1)	1.2e+2 mm	2.9 (0.60 ... 1.9e+2)	12 (-4.9 ... 38)	1.7 (0.68 ... 3.9)	6.4 (-4.2 ... 15)
AFR-44_IPSL-CM5A-MR_r1i1p1_RCA4 (1)	66 mm	0.21 (0.066 ... 1.2)	-13 (-25 ... 1.1)	0.62 (0.020 ... 2.0)	-3.8 (-15 ... 5.3)
AFR-44_MPI-ESM-LR_r1i1p1_CCLM4-8-17 (1)	98 mm	0.48 (0.11 ... 14)	-6.9 (-23 ... 14)	0.93 (0.17 ... 3.2)	-0.66 (-16 ... 10)
AFR-44_MPI-ESM-LR_r1i1p1_RCA4 (1)	95 mm	1.2 (0.30 ... 44)	1.8 (-14 ... 23)	1.9 (0.91 ... 4.3)	6.3 (-0.84 ... 14)

Table 5.1. Event magnitude, probability ratio and change in intensity for 50-year return period for rx5day for observational datasets and each model that passed the evaluation tests, from pre-industrial climate to the present and from the present to 2.6 ℃ above pre-industrial climate.

6 Hazard synthesis

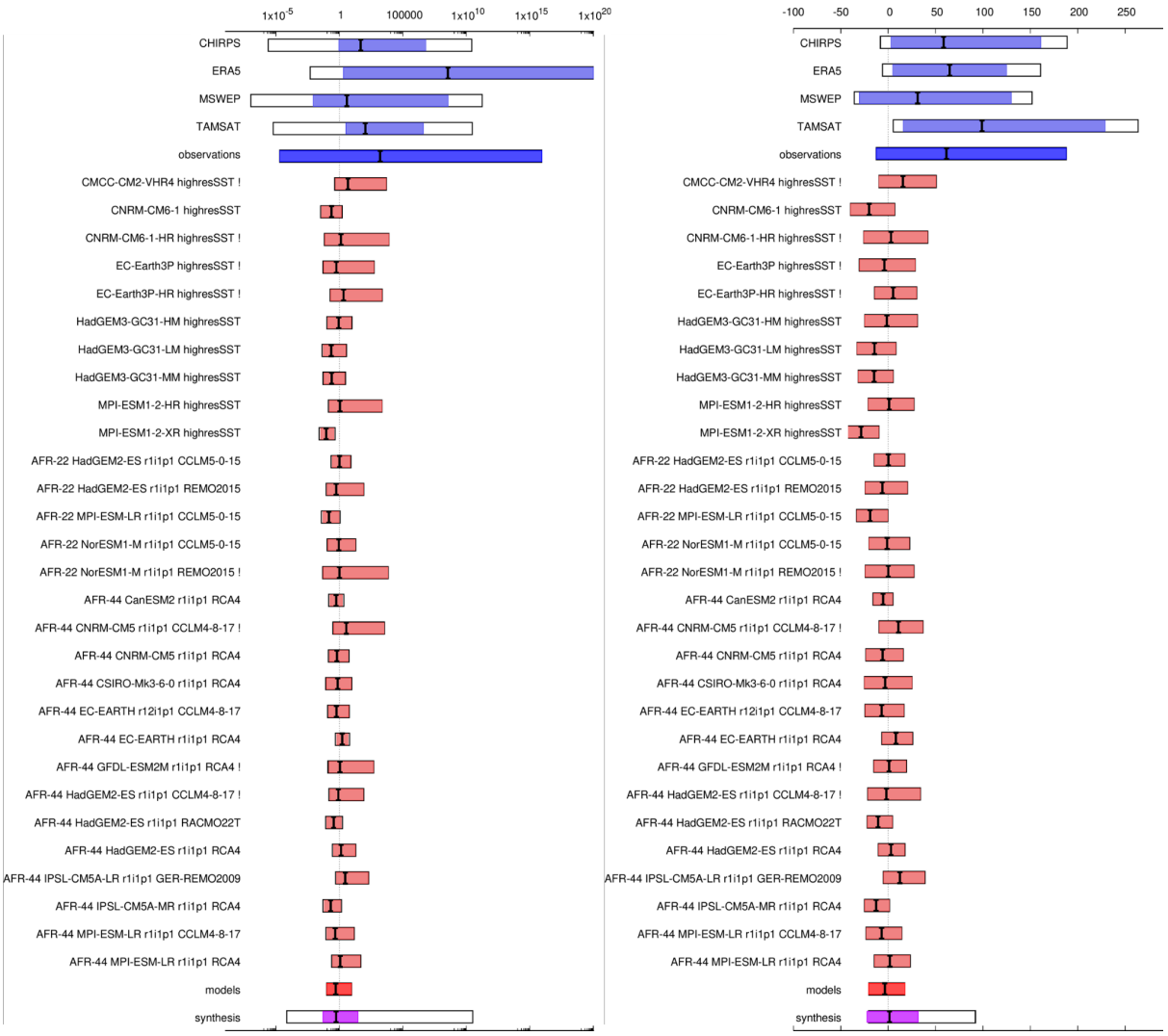

Figure 6.1: *Synthesised changes for a 50-year rx5day event due to GMST. Changes in PR (left) and intensity (right) are shown for a historical period comparing the past 1.3°C cooler climate with the present. If an infinite upper bound has been replaced by a number an exclamation mark has been added to the model name (see Otto et al., 2024).*

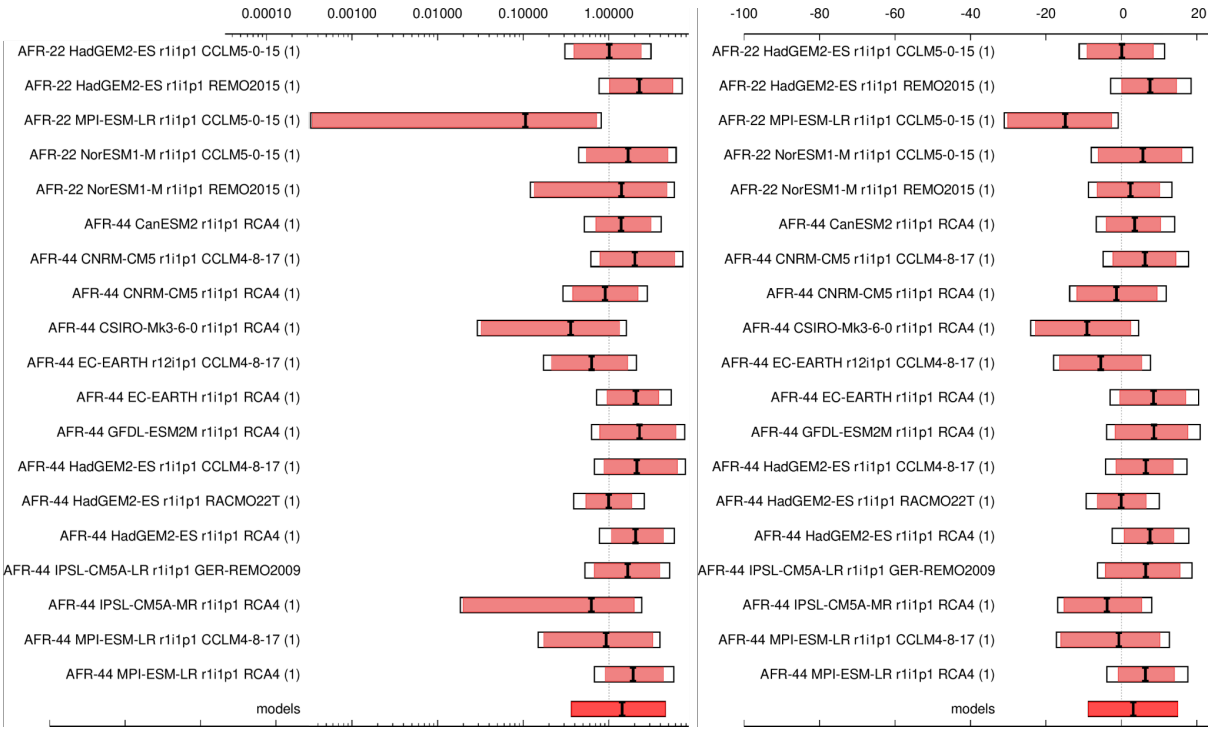

Figure 6.2: *Synthesised changes for a 50-year rx5day event due to GMST. Changes in PR (left) and intensity (right) are shown for a future period, based on model projections only, comparing the present and a 2.6 °C warmed climate.*

For the event definitions described above we evaluate the influence of anthropogenic climate change on the events by calculating the probability ratio as well as the change in intensity using observations and climate models. Models which do not pass the evaluation described above are excluded from the analysis. The aim is to synthesise results from models that pass the evaluation along with the observations-based products, to give an overarching attribution statement.

Figures 6.1 & 6.2 show the changes in probability and intensity for the observations (blue) and models (red). Before combining them into a synthesised assessment, a representation error is added (in quadrature) to the observations, to account for the difference between observations-based datasets that cannot be explained by natural variability. This is shown in these figures as white boxes around the light blue bars. The dark blue bar shows the average over the observation-based products. Next, a term to account for intermodel spread is added (in quadrature) to the natural variability of the models. This is shown in the figures as white boxes around the light red bars. The dark red bar shows the model average, consisting of a weighted mean using the (uncorrelated) uncertainties due to natural variability, plus the term representing intermodel spread (i.e., the inverse square of the white bars).

Observation-based products and models are combined into a single result in two ways. Firstly, we neglect common model uncertainties beyond the intermodel spread that is depicted by the model average, and compute the weighted average of models (dark red bar) and observations (dark blue bar): this is indicated by the magenta bar (Fig. 6.1). The best estimate of the weighted synthesis is given by the black line inside the magenta bar. As, due to common model uncertainties, model uncertainty can be larger than the intermodel spread, secondly, we also show the more conservative estimate of an unweighted, direct average of observations (dark blue bar) and models (dark red bar) contributing 50% each, indicated by the white box around the magenta bar in the synthesis figures. The unweighted best estimate value is not indicated on the plot, but is reported alongside other results (Table 6.1).

Data	Influence of GMST		
		Probability ratio (95% CI)	**Intensity change (%) (95% CI)**
Observations	**Past-Present**	1640 (10^{-5} - 10^{16})	61.6 (-12.5 - 188)
Models		0.51 (0.01 - 8.99)	-3.56 (-20.6 - 17.6)
Synthesis (weighted)		0.55 (0.052 - 29.2)	1.45 (-22.3 - 31.7)
Synthesis (unweighted)		29.01 (10^{-4} - 10^{10})	29.02 (-20.8 - 92.1)
Models only	**Present-Future**	1.43 (0.37 - 4.56)	3.15 (-8.74 - 14.9)

Table 6.1: *Summary of results for 5-day extreme precipitation events over southern Botswana, presented in Figs 6.1 & 6.2: changes due to GMST include past-present changes and present-future changes. Both the weighted and unweighted syntheses are reported. Statistically significant increases (decreases) in probability and intensity are highlighted in dark blue (orange), while non-significant increases are highlighted in light blue (orange).*

As discussed in section 3, the observational results show a very strong increase in the rx5day in the region. When synthesised, the overall probability ratio is more than 1600 and the change in intensity more than 60%, far exceeding Clausius-Clapeyron scaling. These results carry significant uncertainty, however the qualitative result of a strong increase is mirrored across both the larger regional scale and at the local scale, suggesting that it is robust.

The results from models are mixed, with similar numbers of models indicating increases and decreases, and only a single model giving a significant trend in either direction. The magnitude of these changes is also far below that shown in the observations. When synthesised, models give a decrease in likelihood of around 50% and a slight decrease in intensity by around 4% in the 50 year rx5day event, with uncertainty ranges both roughly centred on no change.

When both lines of evidence are synthesised, due to the large number of models and the much lower sampling uncertainty, the weighted synthesis result gives an almost identical result of a decrease in likelihood by 45% and very slight increase in intensity of 1.5%. However, as observations and models fundamentally disagree on the qualitative sign of change, we also report the unweighted result. This suggests a substantial but not statistically significant increase in probability ratio by a factor of 29 and increase in intensity of 29%. This result reflects the very strong observational increase across regional and local scales. Finally, given further 1.3 C of warming, models project an amplification of such extremes, which are expected to increase in frequency by about 40% and in intensity by approximately 3%, though again these results are not significant at the 95% level. This is in contrast to the present day model synthesis, which gives an overall decrease. This discrepancy may result from a combination of at least two factors: i) HighResMIP models are not included in the future projection analysis while they tend to have slightly stronger decreasing trends for the past period, and ii) a genuine emergence of a signal with further warming. Testing the former possibility, we find that

excluding HighResMIP from the present day synthesis results in a less negative trend, which suggests that including it in future would indeed depress the positive signal from CORDEX models alone.

In conclusion, it is challenging to quantify the attributable signal on the rx5day index, but it is clear that the region has observed a very strong increase in similar extremes that cannot be discounted. Given the combination of physical reasoning that warmer air holds more moisture, the strong observed increase in extremes, and the projected shift towards an increase in precipitation with further warming, we conclude that ACC likely amplified the rainfall leading to flooding in southern Botswana, but we cannot confidently quantify by how much.

Clearly, the specific drivers of extremes in the region and the role of ACC in changing the dynamics leading to such events should be studied in greater detail. Furthermore, to fully disentangle the factors leading from extreme rainfall and flooding to impacts, it is also crucial to consider the vulnerability and exposure in the region.

7 Vulnerability and Exposure

Floods rank among the most destructive natural hazards, with far-reaching consequences for human lives, infrastructure, and economic stability (Aloscious, Artuso & Moghadam, 2025; Lehtonen, 2025; Valera & Sharifi, 2025; Acosta-España et al, 2024). While extreme rainfall is the immediate driver of flooding, the scale and severity of its impacts are determined by a combination of hydrological, infrastructural, and socio-economic factors (Singhal et al., 2025; Valera & Sharifi, 2025). Highly vulnerable communities, such as those living in informal settlements or lacking adequate infrastructure, experience disproportionately severe consequences, even from moderate flooding events (Lehtonen, 2025; Valera & Sharifi, 2025). Meanwhile, exposure - measured in terms of population density, built environment, and economic assets in flood-prone areas - determines the extent to which people and infrastructure are affected. The interplay of these factors underscores the importance of integrated flood risk management strategies that address both physical hazards and socio-economic drivers of risk.

Gaborone, Botswana's capital, and the surrounding villages, have occasionally faced seasonal flooding, primarily during the country's rainy season from November to April, mostly when the seasons are wetter than normal (Mutize, 2015; Madzudzo et al, 2018). The city's flat topography, rapid urbanization, and infrastructure constraints have contributed to increasing flood risks, exacerbated by extreme rainfall events (Samuel et al, 2022). In recent years, floods have intensified, with the February 2025 floods standing out as one of the most severe in Gaborone's recorded history (see the flood extent in figure 7.1). Heavy rainfall overwhelmed stormwater drainage systems, leading to widespread inundation of residential areas, roads, and public services. The overflowing Gaborone Dam, which peaked at 105.19% capacity, further exacerbated the crisis, leading to significant displacement, infrastructure damage, and loss of life (Africa Press, 2025). Many communities have lost access to safe water, putting them at risk of disease. Authorities have temporarily shut schools and blocked roads, rerouting traffic to Namibia due to border closures between Botswana and South Africa (Windhoek Observer, 2025). The floods have resulted in the evacuation of 1,806 people (Dube, 2025). The urban poor and communities in low-lying areas have been particularly affected, highlighting the role of socio-economic disparities in flood vulnerability. Further, beyond direct flood impacts, cascading effects such as waterborne disease outbreaks, transportation disruptions, and economic losses compound the disaster's severity (Lowe et al., 2013; Yin et al., 2022).

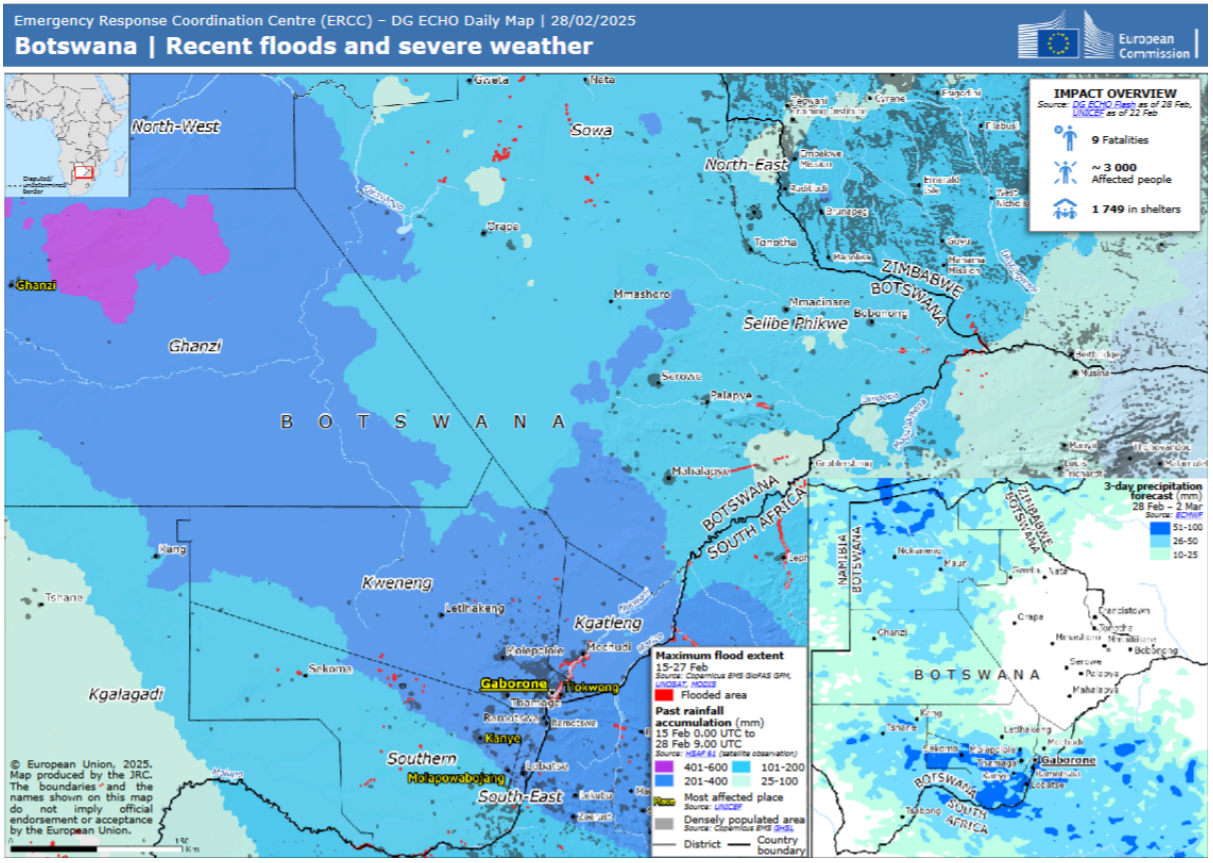

Figure 7.1. *Flood extent map in Botswana as of 28 February, where the capital, Gaborone, is marked in yellow. Sources: DG ECHO, UNOSAT, HSAF, UNICEF & JRC-GHSL via ERCC (2025).*

This analysis explores key dimensions of vulnerability and exposure, including land use, urban planning, disaster management, and policy, to assess the factors that influence the scale of the crisis.

7.1 Land-use, Urban planning and Informality

Gaborone's urban expansion has been largely guided by government-led land-use planning, ensuring relatively low levels of informal settlement - 10% in the city, compared to a 14% national average (UN Habitat, 2018). Most residents have access to essential services, including water (95%), sanitation (85%), electricity (87%), and waste collection (99%) (UN Habitat, 2018). However, vulnerabilities persist in specific areas due to drainage challenges and encroachment on flood-prone land.

Satellite imagery indicates that the February 2025 floods significantly impacted buildings near the Notwane River in southeastern Gaborone, with 670 structures affected (see figure 7.2). Among the displaced population, children and older adults were identified as particularly vulnerable (UNOSAT, 2025). Tlokweng, a repeatedly flood-affected area, continues to experience drainage issues, exacerbating local risks (Federal Ministry of Economic Cooperation and Development Germany, 2024). Additionally, disruptions to road networks and power supply have hampered mobility and access to essential services, with health clinics in Molapowabojang and Kanye reporting service interruptions (UNICEF, 2025).

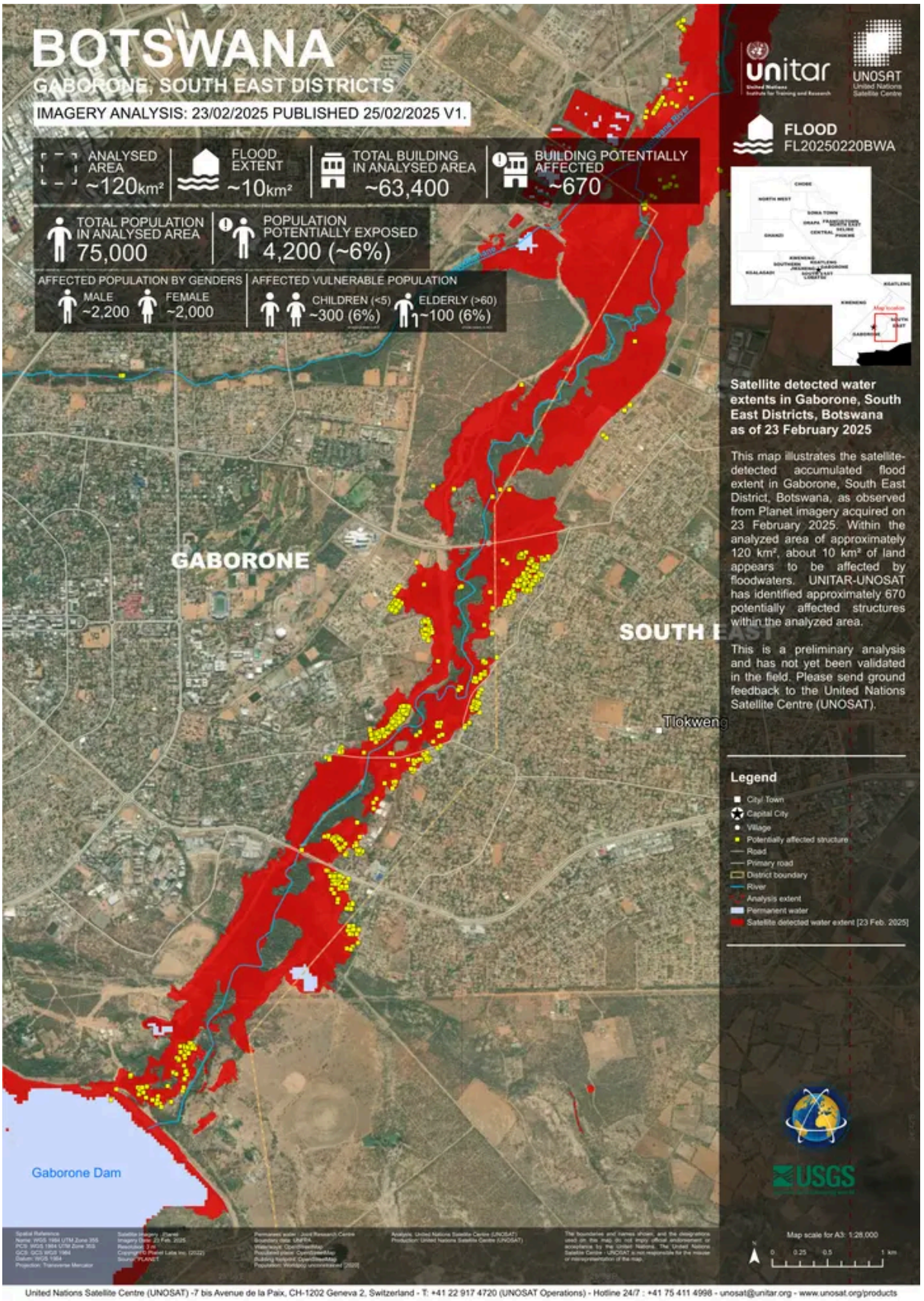

Figure 7.2. *Flood extent map in Gaborone, Botswana, as of 23 February. Source: UNOSAT (2025).*

Land-use changes further contribute to increased flood risks. Between 1984 and 2022, built-up areas in the Notwane watershed, which includes Gaborone, expanded from 0.04% to 9.20%, while agricultural land and natural vegetation declined significantly (Magidi et al., 2024). Projections for the Gaborone Dam catchment indicate a continued reduction in shrubland and tree savanna, alongside an increase in built-up areas and bare land, which may lead to higher runoff and lower filtration rates (Matlhodi et al., 2021). These trends underscore the importance of integrating climate resilience into future urban planning.

Recognizing these challenges, urban drainage improvements are underway through initiatives like the GIZ Resilience Initiative Africa and Connective Cities program, which includes Tlokweng and Gaborone in its urban drainage master plan (GIZ, 2023). The effective implementation of such strategies, as well as stricter land-use regulations and improved stormwater management (Madzudzo, Toteng & Mulalu, 2018; Gunanada & Koestoer, 2023), will be crucial in mitigating future flood risk.

Urban expansion and infrastructure have played a crucial role in shaping flood risks, but mitigating these risks requires a broader approach that includes early warning systems, preparedness, and disaster response.

7.2 Flood Risk Management

The February floods in and around Gaborone exposed key challenges in flood risk management. While the Botswana Department of Meteorological Services (DMS) issued a rainfall warning on February 14th, and forecasted heavy rainfall for the following day, the country lacks a fully functioning Flood Early Warning System (FEWS) (Gunanada & Koestoes, 2023; Samuel et al., 2022). Although efforts have been made to enhance disaster management, current strategies remain largely response-driven, with opportunities to further integrate and strengthen proactive measures (Gunanada & Koestoes, 2023).

Enhancing public access to flood risk information remains an important consideration. While disaster response strategies engage key institutional stakeholders such as the police, military, and health workers, expanding broader community engagement in flood preparedness could further strengthen resilience (Gunanada & Koestoes, 2023). Additionally, flood risk management policies could benefit from deeper integration into urban planning, infrastructure development, and land-use policies. Greater coordination between the national disaster management office, urban planning entities, and water management agencies could help ensure a more cohesive and effective flood mitigation strategy (Gunanada & Koestoes, 2023). Rapid urbanization, particularly the expansion of informal settlements in flood-prone areas, presents an additional challenge requiring attention (Madzudzo, Toteng & Mulalu, 2018).

The absence of a centralized flood data repository limits authorities' ability to assess flood patterns, identify high-risk zones, and develop data-driven risk reduction strategies. Without structured historical records on flood frequency, severity, and impacts, improving forecasting models and early warning capabilities remains challenging (Madzudzo, Toteng & Mulalu, 2018). The unprecedented nature of the February 2025 floods, described as the most severe disaster in Gaborone in 60 years (Mmegionline, 2025), could mean that most people do not remember a similar event in their lifetimes, further emphasizing the need for institutionalized knowledge to inform preparedness and response

strategies. Strengthening institutional memory of past disasters would enhance preparedness, response strategies, and long-term resilience planning.

Gaps in flood risk management highlight the need for stronger disaster response mechanisms and policy frameworks that address immediate and long-term flood resilience.

7.3 Disaster Management and Flood Policy

While Botswana is highly flood-prone, it is also at high risk of droughts and therefore, historically, there has been an outsized focus on drought mitigation in Botswana, with a comprehensive National Drought Management policy and investments in early warning and improving water infrastructure in drought-prone areas (SADRI, n.d.). The National Disaster Management Framework includes a National Disaster Policy from 1996 and a National Disaster Risk Management Plan (2009), however, a comparative evaluation of these policies found that they were partially out of date, not reflecting current climate-related flood risks and requiring additional public input (Gunanada & Koestoer, 2023). Further research indicates that low technology uptake for responding to flood disasters and lack of proactive guidelines indicates that the national management strategy, plan, and policy require updating (Samuel et al., 2022).

Botswana submitted its national climate action plan, Nationally Determined Contributions (NDC), in 2024 that includes a focus on adaptation. The NDC acknowledges the country's vulnerability to floods and particularly their impact on nearly all infrastructure in the country and human lives (Botswana NDC, 2024). They prioritised adaptation measures such as improving drainage systems and their maintenance, using climate-resilient building materials and an expande d multi-hazard Early Warning System (Botswana NDC, 2024). The country stressed that it would prioritize its limited financial resources towards adaptation, given it is amongst the lowest emitters of greenhouse gases worldwide (Botswana NDC, 2024).

V&E Conclusions

The February floods in Botswana highlighted how extreme rainfall interacts with infrastructure, land-use, urban development, and socio-economic disparities to shape disaster impacts. While government-led land use planning has contributed to lower informality and high access to essential services, flood risk remains significant due to encroachment into flood-prone areas and insufficient drainage systems. The expansion of built-up areas and the simultaneous decline in vegetation have further contributed to increased runoff and reduced water infiltration, exacerbating flood risk.

Infrastructure not designed to withstand such extreme rainfall resulted in overwhelmed roads, drainage networks, and health facilities. Given the country's reliance on both boreholes (56%) and dams (44%) for water supply, resilient infrastructure planning must address vulnerabilities to both floods and droughts. While efforts to improve drainage, land-use regulation, and disaster preparedness are ongoing, expanding coning enforcement and early warning systems will be key. A comprehensive approach that integrates multi-hazard assessment into urban planning, infrastructure investment, and disaster management will help strengthen resilience to future extreme weather events.

Data availability

All time series used in the attribution analysis are available via the Climate Explorer.

References

All references are given as hyperlinks in the text.

Appendix

A.1 Observed trends and statistical models

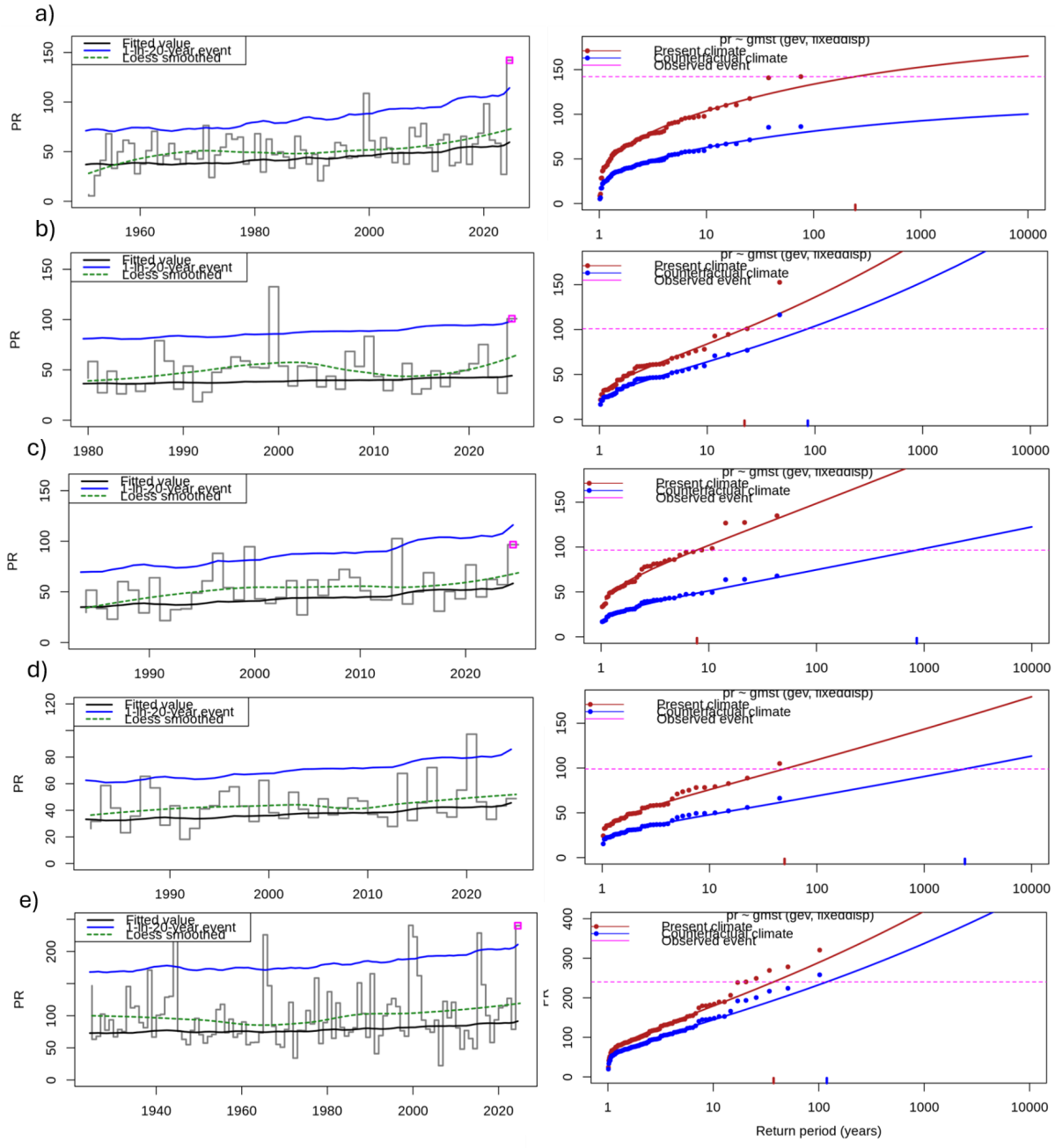

Figure A.1: *Trends (left) and return period plots (right) for each gridded observational dataset: a) ERA5, b) MSWEP, c) TAMSAT, d) CHIRPS, e) Weather station. On (a-c, e) the 2025 event is shown by a pink square (left) and a pink dashed line (right). On (d), the pink dashed line shows the magnitude of the 50-year event.*

A.2 Model evaluation figures

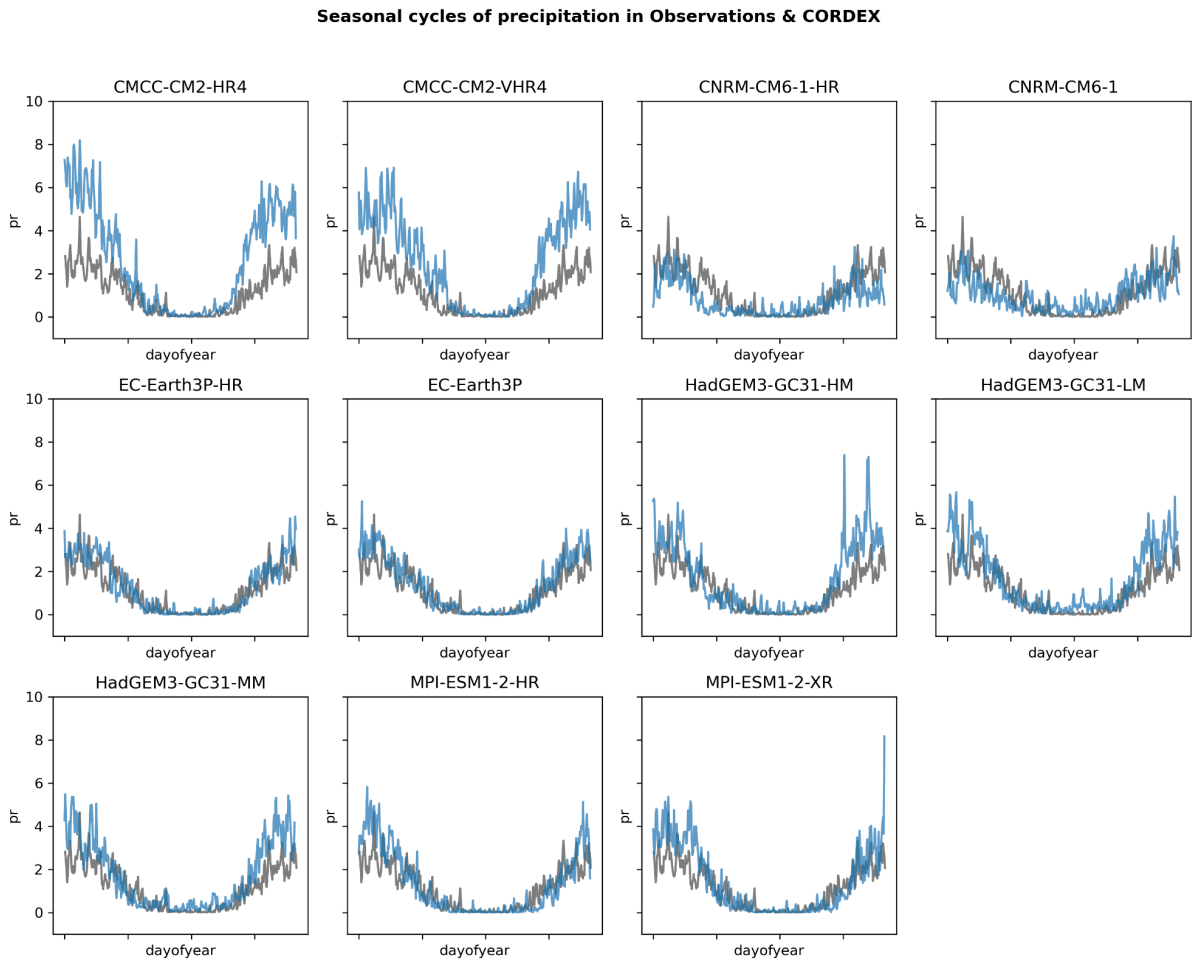

Figure A.2: *Seasonal cycles of precipitation in observations (MSWEP), shown in black, and HighResMIP models, shown in blue.*

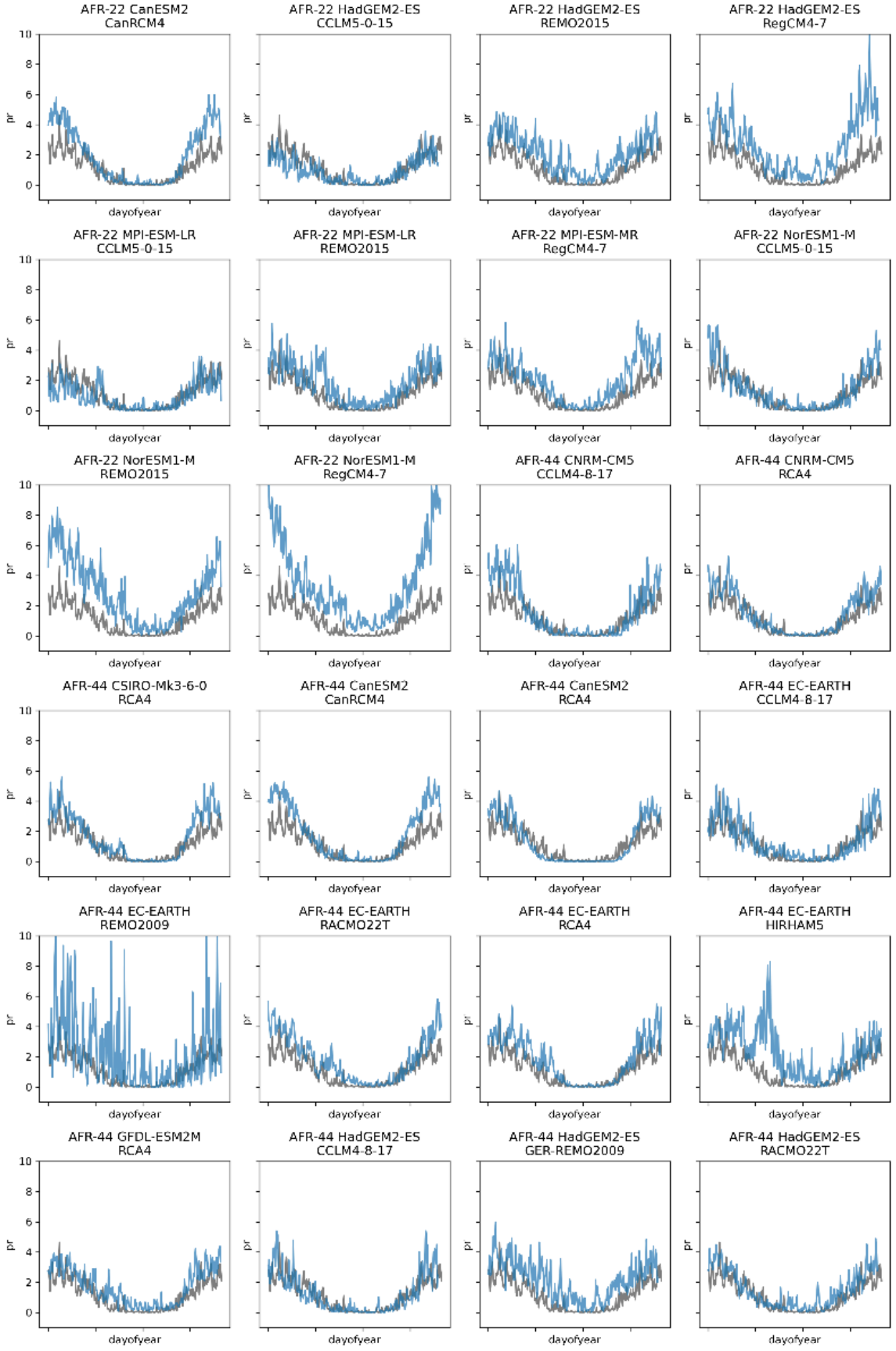
AFR-22 CanESM2
CanRCM4
AFR-22 HadGEM2-ES
CCLM5-0-15
AFR-22 HadGEM2-ES
REMO2015
AFR-22 HadGEM2-ES
RegCM4-7
AFR-22 MPI-ESM-LR
CCLM5-0-15
AFR-22 MPI-ESM-LR
REMO2015
AFR-22 MPI-ESM-MR
RegCM4-7
AFR-22 NorESM1-M
CCLM5-0-15
AFR-22 NorESM1-M
REMO2015
AFR-22 NorESM1-M
RegCM4-7
AFR-44 CNRM-CM5
CCLM4-8-17
AFR-44 CNRM-CM5
RCA4
AFR-44 CSIRO-Mk3-6-0
RCA4
AFR-44 CanESM2
CanRCM4
AFR-44 CanESM2
RCA4
AFR-44 EC-EARTH
CCLM4-8-17
AFR-44 EC-EARTH
REMO2009
AFR-44 EC-EARTH
RACMO22T
AFR-44 EC-EARTH
RCA4
AFR-44 EC-EARTH
HIRHAM5
AFR-44 GFDL-ESM2M
RCA4
AFR-44 HadGEM2-ES
CCLM4-8-17
AFR-44 HadGEM2-ES
GER-REMO2009
AFR-44 HadGEM2-ES
RACMO22T
pr
dayofyear
0
2
4
6
8
10

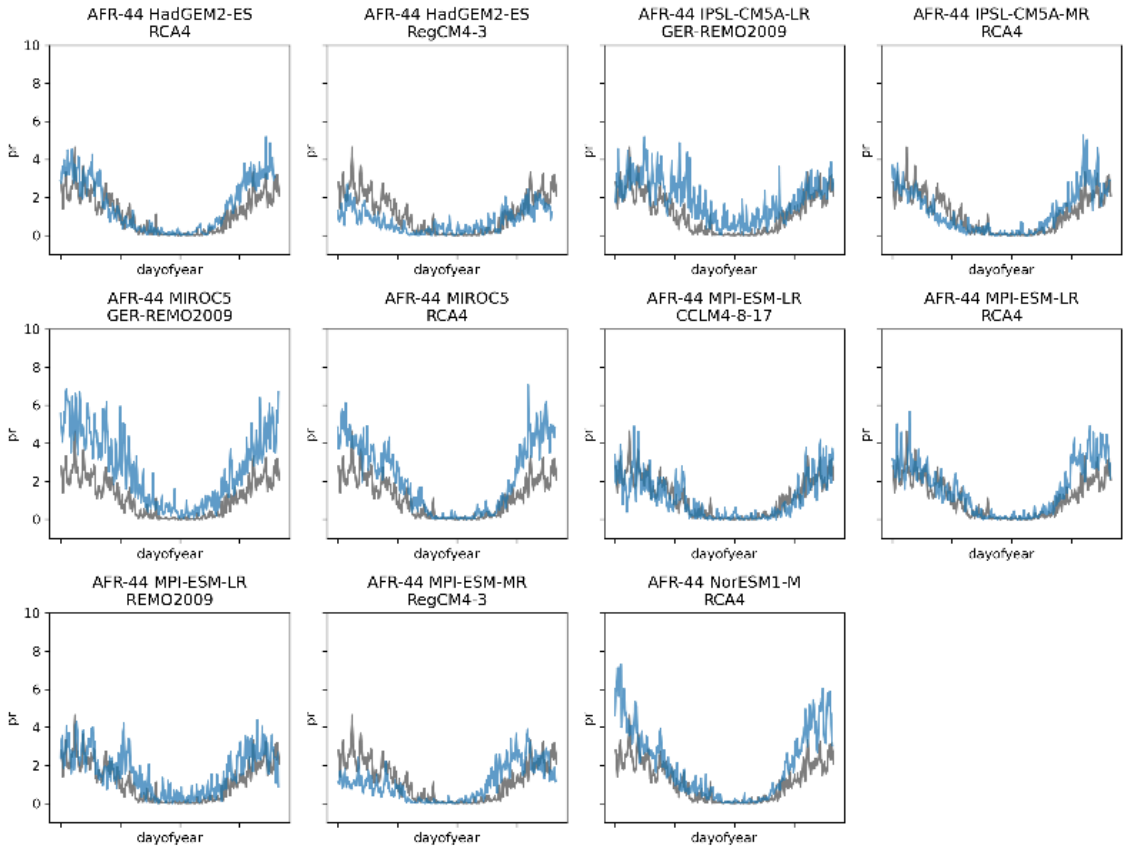

Figure A.3: *Seasonal cycles of precipitation in observations (MSWEP), shown in black, and CORDEX models, shown in blue.*

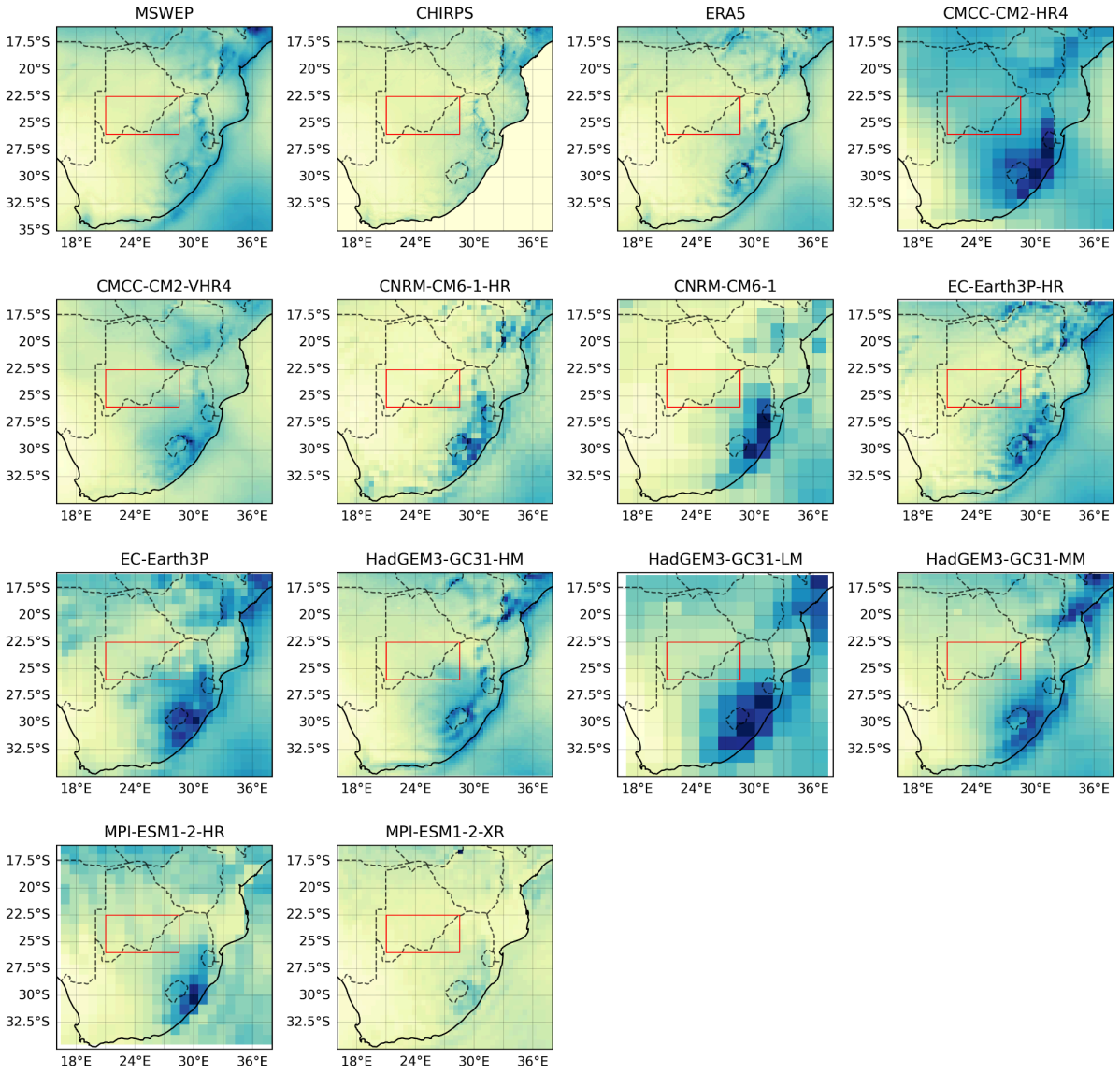

Figure A.4: *Spatial patterns of annual precipitation in observations and HighResMIP models. The study region for the rainfall analysis is highlighted in red.*

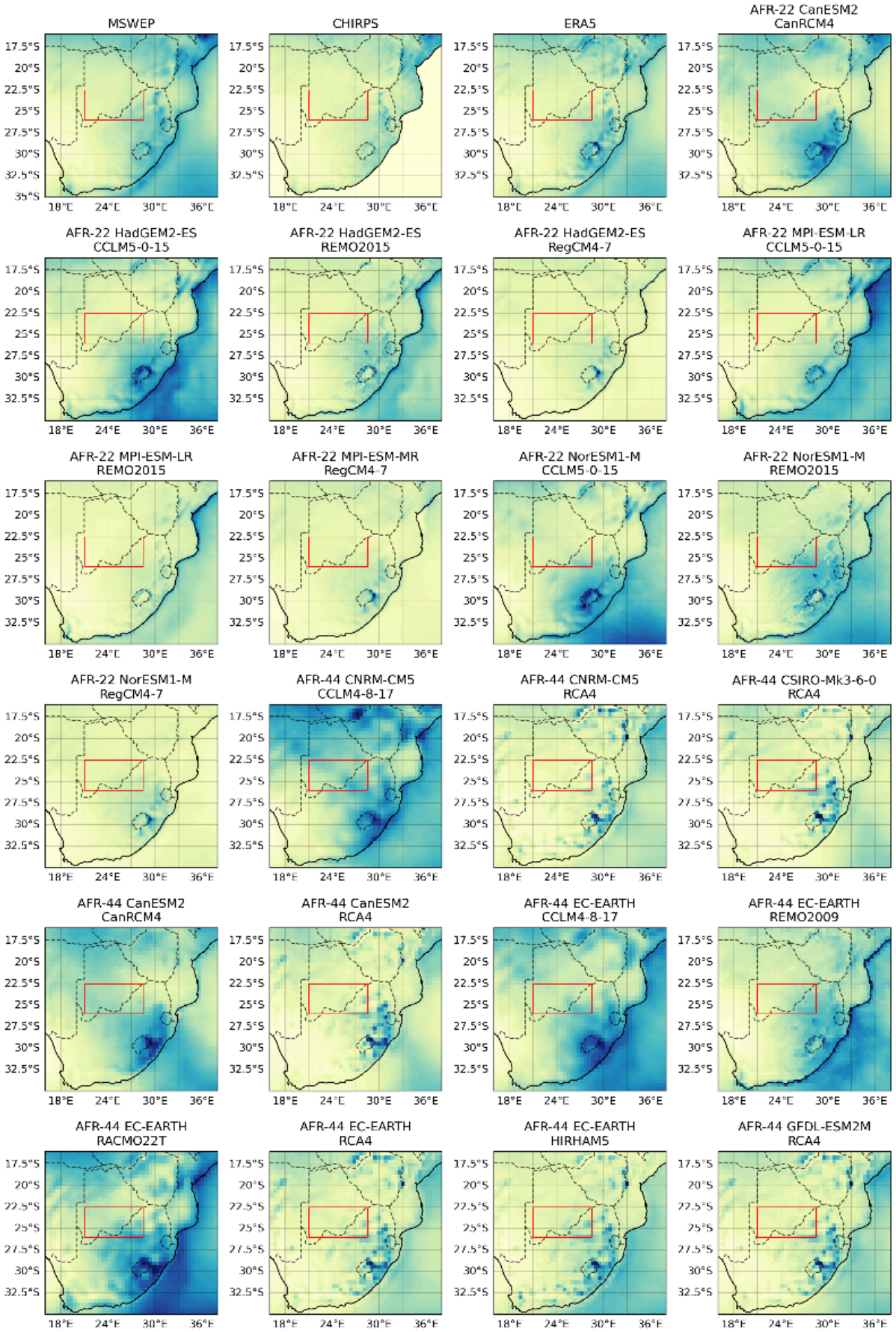
MSWEP
CHIRPS
ERA5
AFR-22 CanESM2
CanRCM4
AFR-22 HadGEM2-ES
CCLM5-0-15
AFR-22 HadGEM2-ES
REMO2015
AFR-22 HadGEM2-ES
RegCM4-7
AFR-22 MPI-ESM-LR
CCLM5-0-15
AFR-22 MPI-ESM-LR
REMO2015
AFR-22 MPI-ESM-MR
RegCM4-7
AFR-22 NorESM1-M
CCLM5-0-15
AFR-22 NorESM1-M
REMO2015
AFR-22 NorESM1-M
RegCM4-7
AFR-44 CNRM-CM5
CCLM4-8-17
AFR-44 CNRM-CM5
RCA4
AFR-44 CSIRO-Mk3-6-0
RCA4
AFR-44 CanESM2
CanRCM4
AFR-44 CanESM2
RCA4
AFR-44 EC-EARTH
CCLM4-8-17
AFR-44 EC-EARTH
REMO2009
AFR-44 EC-EARTH
RACMO22T
AFR-44 EC-EARTH
RCA4
AFR-44 EC-EARTH
HIRHAM5
AFR-44 GFDL-ESM2M
RCA4

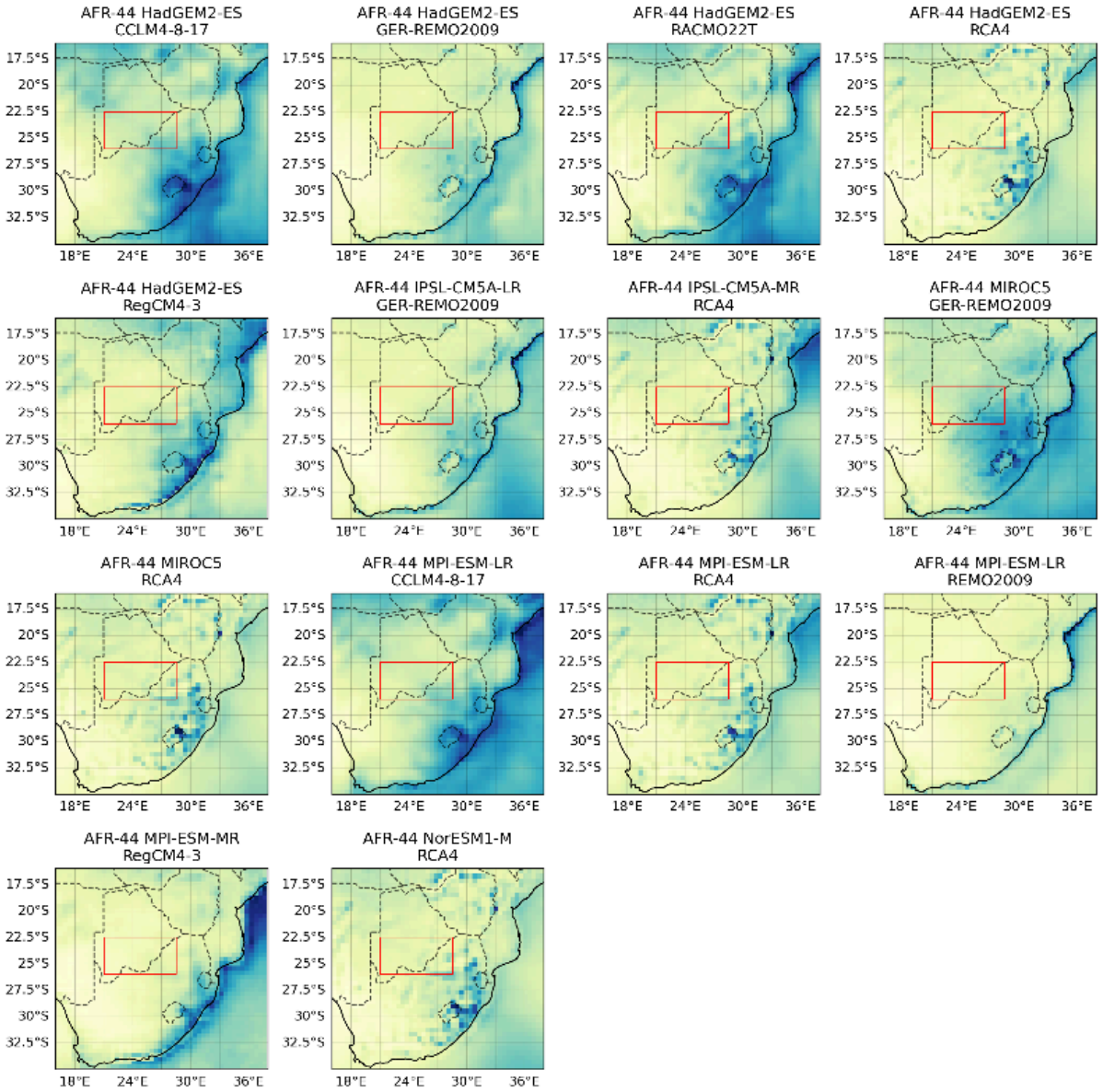

Figure A.5: *Spatial patterns of annual precipitation in observations and CORDEX models. The study region for the rainfall analysis is highlighted in red.*